INTERNATIONAL JOURNAL FOR NUMERICAL METHODS IN ENGINEERING

Int. J. Numer. Meth. Engng 0000; **00**:2–27

Published online in Wiley InterScience (www.interscience.wiley.com). DOI: 10.1002/nme

A Domain-Decomposition Strategy for a Compressible Multiphase Flow Interacting with a Structure

M. Greco[1,2,3,*], G. Colicchio[1,2] and O.M. Faltinsen[2,3]

[1] *CNR-INSEAN, The Italian Ship Model Basin, via di Vallerano 139, 00128 Roma - Italy.* [2] *AMOS, NTNU, Trondheim - Norway.* [3] *Dept. of Marine Technology, NTNU, Trondheim - Norway*

SUMMARY

The problem of a high-pressure gas cavity and its interaction with surrounding liquid and a close by structure is examined numerically. Even Though this is of interest in many practical applications; here the focus is on an underwater explosion. A one-way domain-decomposition (DD) strategy coupling a radial and a 3D solver for compressible multi-phase flows is proposed and the different components are successfully verified. This is a time-space DD that assumes the explosion occurs sufficiently far from boundaries. It means that the radial solution is used everywhere until radial symmetry is applicable. When acoustic waves reach a close structure, the radial solution initiates the 3D solution near the body and continues to be applied only far from the structure and to provide the boundary conditions for the 3D sub-domain. The advantage is to limit the computational costs and preserve reliability and accuracy. The radial solution could be applied to assess local damages during the initial acoustic phase; the time-space DD needs to be used to investigate both local and global consequences on the vessels. The structure is modelled both as a rigid wall and as a orthotropic plate which provides a good representation of the bottom grillages of ships. Copyright © 0000 John Wiley & Sons, Ltd.

Received . . .

KEY WORDS: Gas cavity; compressible two-phase flow; wave-structure interaction; domain decomposition

1. INTRODUCTION

Several practical examples exist where gas cavities with initially high pressure evolve in time affecting the surrounding liquid and inducing relevant loads on close structures. A military application is represented by underwater explosions. They have been recognized as one of the main causes for losses of US navy ships in the last sixty years (see [1]) and are an issue both for ships and offshore structures. This highlights the need for proper predictions of the induced structural effects and for improvement of vessel design. For this reason several physical tests were performed along the years, most of them not publicly available, and theories were developed (see [2]). Another dangerous scenario is given by shock waves caused by implosion of cavitating bubbles near hydraulic machinery which can cause erosion of the structure (see [3]). The same phenomena can lead to positive outcomes in rather different contexts. Underwater explosions seem to be an effective technique to improve the harvest in cold countries. The resulting shock waves crush the ice block covering the soil and enlarge the sunshine duration (see [4]). Another positive outcome is represented by implosion of micro-bubbles with ultrasound in biological flows. This is used in medical field as a noninvasive technique to remove calculi in human bodies (see [5]). All these problems share similar features: a high-pressure cavity oscillates immersed in liquid and generates acoustic waves. These can interact with sufficiently close structures and can be totally reflected—-partially reflected and partially transmitted in the solid. The wave-body interaction can cause elastic or plastic deformations or even the rupture of the material. The reflected waves can go back to their source, *i.e.* the gas cavity, and interact with it (see sketch in figure 1). These phenomena might lead to cavitation. During these initial stages compressibility matters both in the gas and liquid phases, while later on the strength of the acoustic wave reduces and the compressible effects remain important only for the cavity while the liquid can be considered incompressible. This means a two-phase 3D solver can be used coupling an incompressible liquid with a compressible bubble, as it

*Correspondence to: CNR-INSEAN, via di Vallerano 139, 00128 Roma - Italy or AMOS/NTNU, O. Nielsens vei 10, 7491 Trondheim - Norway. E-mail: marilena.greco@cnr.it; marilena.greco@ntnu.no

Prepared using nmeauth.cls
DOI: 10.1002/nme

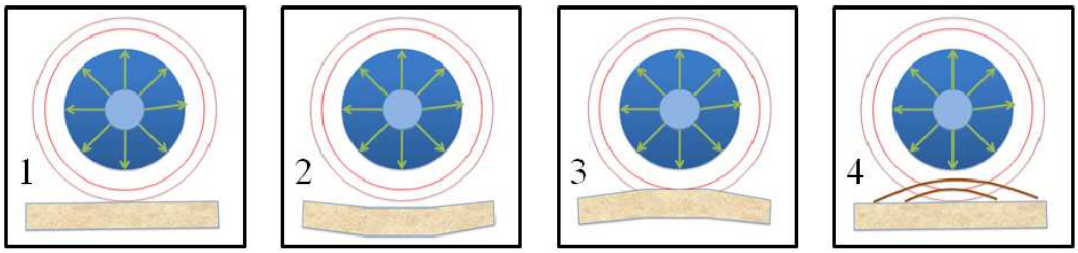

Figure 1. Main phenomena during the evolution of a high-pressure cavity in a liquid: 1) bubble oscillations with acoustic waves moving out of the bubble, 2) and 3) interaction with a structure can cause deformations and damages, 4) reflected waves from the body can interact with the cavity.

has been presented in [6]. There, the flow evolution and induced body loads in this stage have been studied in the case of water shipping with plunging wave hitting the vessel deck and entrapping a cavity. Here the more complex phenomena involved in the initial stages are considered. Preliminary results reported in [7] and [8] are combined and widened for a more comprehensive documentation of the research activity. The aim is to develop a solver able to investigate cavity evolution from the acoustic phase until the cavity oscillation phase and so able to assess possible local and global consequences on the structures.

Despite being a sensitive research topic, underwater explosions can provide more reference results for verification and validation of the solver. Therefore it is the scenario considered as application in the present work. An underwater explosion induces a chemical reaction and a detonation process and these are responsible for the formation of a hot gas with high pressure and the release of a shock wave traveling in the surrounding fluid. The formed superheated, spherical, bubble will quickly expand, reducing the inner high pressure until a maximum radius is reached. After that, the bubble starts to oscillate and induces oscillations in the pressure of the surrounding liquid. In the first stage (shock wave) both gas and the surrounding liquid behave as compressible, in the later stages (gas bubble) the acoustic wave will disappear in time and the water can be considered more and more incompressible. The interaction of this two-phase fluid with a body will then depend on the closeness of the body to the explosion zone and by the presence or less of other boundaries, *e.g.* the sea floor, the free surface.

Prepared using nmeauth.cls
DOI: 10.1002/nme

Here we study the problem after the chemical-reaction and detonation stages and study numerically the compressible cavity in a generally compressible liquid. A numerical solution strategy is proposed as a compromise between capability in handling the mechanisms governing the evolution and efficiency. It is characterized by a time-space zonal approach coupling two compressible solvers: a radial solver and a 3D method. The former is used in the whole domain as long as the acoustic waves do not reach any boundary and radial symmetry is preserved. The latter is switched on near the boundaries (near a structure in the present application) and receives boundary conditions from the radial solver still used far from the boundaries. The DD is aimed to investigate the problem in all stages: 1) initial acoustic phase with compressible effects everywhere, 2) cavity-oscillation phase with liquid compressibility reducing in time 3) cavity collapse near or onto a structure.

The two solvers, the domain-decomposition strategy and the orthotropic plate model adopted to simulate the bottom of a ship are described in section 2. There, some relevant verification studies are also provided for the radial solution in infinite fluid domain and for the incompressible added mass of the plate. In section 3, underwater explosions interacting with structures are examined. The radial solution is applied for an underwater explosion in an infinite fluid and then a plate is introduced to assess the induced stresses and deformations on the structure. The time-space domain decomposition is applied next to verify its robustness and accuracy in the case of an underwater explosion near a rigid wall. In the last section the main conclusions are drawn and future steps are indicated.

2. NUMERICAL SOLVER

The examined problem is of great interest but rather complicated because it involves at least two fluids, with different properties, and a generally deformable structure, able to affect the surrounding fluid. The latter means that hydroelasticity can be excited. The different features of the proposed solution algorithm can be described as follows.

Prepared using nmeauth.cls
DOI: 10.1002/nme

2.1. 3D solution: compressible solver for multi-phase flows

Assuming a Cartesian Earth-fixed coordinate system (x, y, z), the governing equation of the problem can be formally written as

$$\frac{\partial \boldsymbol{U}}{\partial t} + \nabla \cdot \boldsymbol{F} = 0\,, \tag{1}$$

with $\boldsymbol{U} = [u, \rho u, \rho v, \rho w, E]^T$ and $\boldsymbol{F}$ with components $F_x = [\rho u, \rho u^2 + p, \rho uv, \rho uw, (E + p)u]^T$, $F_y = [\rho v, \rho uv, \rho v^2 + p, \rho vw, (E + p)v]^T$ and $F_z = [\rho w, \rho uw, \rho vw, \rho w^2 + p, (E + p)w]^T$; moreover (u, v, w) is the velocity vector, p the pressure and E the total energy $\rho[e + (u^2 + v^2 + w^2)/2]$. For the closure of the problem we need an equation of state (EOS) for the specific internal energy e. Here this is assumed of the form $\rho e = f_f(\rho)p + g_f(\rho)$, with the functions f_f and g_f depending on the fluid (indicated by the subscript f) properties. In particular, the JonesWilkinsLee EOS is used for the gas generated by the explosion (see [9]) and an isentropic Tait relation for the water (see [2]), *i.e.*

$$\begin{aligned} &f_g = 1/\omega \qquad g_g = [-A_g(1 - \omega\rho_g/(R_1\rho_{0g}))e^{-R_1\rho_{0g}/\rho} - B_g(1 - \omega\rho_g/(R_2\rho_{0g}))e^{-R_2\rho_{0g}/\rho_g}]/\omega \\ &f_w = 1/\gamma_w \quad g_w = (B_w - A_w)\gamma_w/(\gamma_w - 1) \end{aligned} \tag{2}$$

Here the subscripts g and w stand for gas and water, respectively, ρ_{0g} is the initial gas density, γ_w is the ratio of specific heats for water and the other quantities are parameters given later and depend on the properties and initial conditions for the two fluids soon after the explosion.

Equation (1) is solved numerically with a second-order finite-difference scheme in space and integrated in time with a Total Variation Diminishing (TDV) third-order Runge-Kutta scheme (see *e.g.* [10]). This is suitable for solving hyperbolic conservation laws with stable spatial discretization and ensures suitable accuracy in long-time simulations with relatively limited computational costs. The fluxes in the governing equation are solved using a MUSCL scheme which is a second-order accurate extension of Godunov's method (see *e.g.* [11]).

A level set function ϕ is used to represent implicitly the interface between the two fluids and it is advected in time using the equation

$$\frac{\partial \phi}{\partial t} + \boldsymbol{V}_i \cdot \nabla \phi = 0 \tag{3}$$

Prepared using nmeauth.cls
DOI: 10.1002/nme

where $\boldsymbol{V}_i$ is the interface velocity calculated as in [12]. Across the interface a Riemann problem must be solved to ensure proper reflection and transmission of shock waves during the evolution. This is locally a 1D problem in the normal direction of the interface and is formally the same as for the interface condition in the radial symmetric problem explained in section 2.2.

To make the solution efficient in time, an adaptive mesh refinement is used according to [13]. The grid is halved either close to the interface between the two fluids or in proximity of high gradients of the fluid variables $\boldsymbol{U}$. An example of mesh refinement is shown in the left of figure 2, at the starting time of the explosion. Close to the interface the grid size is extremely refined, while the

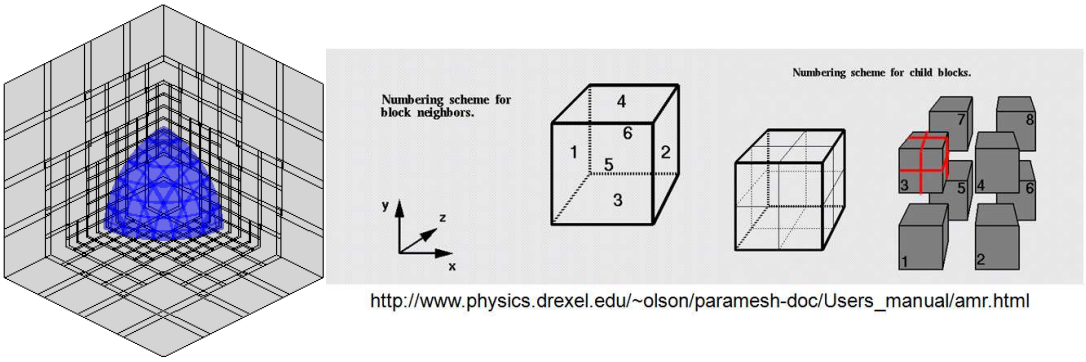

Figure 2. Left: example of adaptive mesh refinement close to the gas-water interface. Right: algorithm for the dynamic refinement.

refinement grades to a coarse mesh far from the interesting region. The adaptive-mesh algorithm can be described as follows: the grid is split in blocks (see on the right of the figure) and each block can be successively split in eight blocks so that the local grid size dynamically changes and ensures proper refinement where necessary. To achieve this a variable of interest is monitored, for example the pressure. If this becomes larger than a certain threshold value, for example in block 3 of figure 2, then the block is split in eight blocks and the check is repeated on each of the new blocks so that further refinement is introduced if necessary. At the same time the grid becomes coarser in time where the flow variations are not significant.

Prepared using nmeauth.cls
DOI: 10.1002/nme

In many situations one can expect that the explosion occurs very far from other boundaries and that hydrostatic pressure does not affect the explosion phenomenon. This leads to a radial symmetry of the bubble evolution and to the opportunity to simplify the problem as '1D' in the radial direction, as explained next.

2.2. '1D' radial solution: compressible solver for multi-phase flows

We assume to study the problem just after the chemical reactions and the detonation phase have occurred, so the initial values of bubble radius, density and pressure, need to be obtained from physical tests or extracted from empirical formulas identified along the years of research in this field (see *e.g.* [2]). A compressible '1D' solver along the radial direction r is then used to simulate the flow evolution in an infinite domain. Assuming radial symmetry, the multi-dimensional governing equation (1) reduces to a one-dimensional Euler equation in the r direction of the form

$$\frac{\partial \boldsymbol{U}}{\partial t} + \frac{\partial \boldsymbol{F}}{\partial r} = \boldsymbol{S}\,, \tag{4}$$

with $\boldsymbol{U} = [\rho, \rho u, E]^T$, $\boldsymbol{F} = [\rho u, \rho u^2, (E+p)u]^T$ and $\boldsymbol{S} = 2[\rho u/r, \rho u^2/r, u(E+p)/r]^T$. Here u is the radial velocity, p the pressure and E the total energy $\rho(e + u^2/2)$. The same EOSs as in the 3D case are used for the specific internal energy e to close the problem for gas and water.

The problem is solved in time with a first order scheme and using the Harten-Lax-Van Leer (HLL) approximate Riemann solver (see [14]) to estimate the fluxes $\boldsymbol{F}$ in each fluid and enforcing a two-shock approximation to the Riemann problem at the interface as proposed in [12]. The latter provides an exact solution when a shock wave is reflected and is reliable for gas-gas or gas-water flow. This is given by solving for the two nonlinear characteristics intersecting at the interface and using mass and momentum jump conditions for the transmitted and reflected shock. The resulting equation system is nonlinear and is solved iteratively with a Newton-Raphson method giving u_i, p_i, ρ_i^L and ρ_i^R, respectively, the radial velocity and pressure at the interface and the left and right density. To avoid possible instability of the solution, the left and right densities are corrected by enforcing an isobaric condition across the interface. This interface algorithm is inserted into a ghost fluid method (see [12]) providing the conditions across the interface to each fluid. In particular, let

Prepared using nmeauth.cls
DOI: 10.1002/nme

us assume that the interface is between node i and i+1 of the computational grid and that we need to solve for the fluid on the left. Here we consider that for the nodes $\geq$ i the density, velocity and pressure are, respectively, ρ_i^L , u_i and p_i, and the other needed quantities are obtained in accordance. A similar technique is used when solving for the fluid on the right. At this stage the fluxes $\boldsymbol{F}$ can be calculated in each fluid and the problem can be stepped forward in time. The location of the interface is updated using the velocity u_i.

The solver has been satisfactorily verified against several numerical solutions, for fully 1D problems (in this case $\boldsymbol{S} = 0$ in equation (4)) and problems with radial symmetry and showed to be accurate also in later stages of the evolution. For this reason, there has been no attempt to implement a second-order temporal scheme. Examples of comparisons are given in figure 3. The use

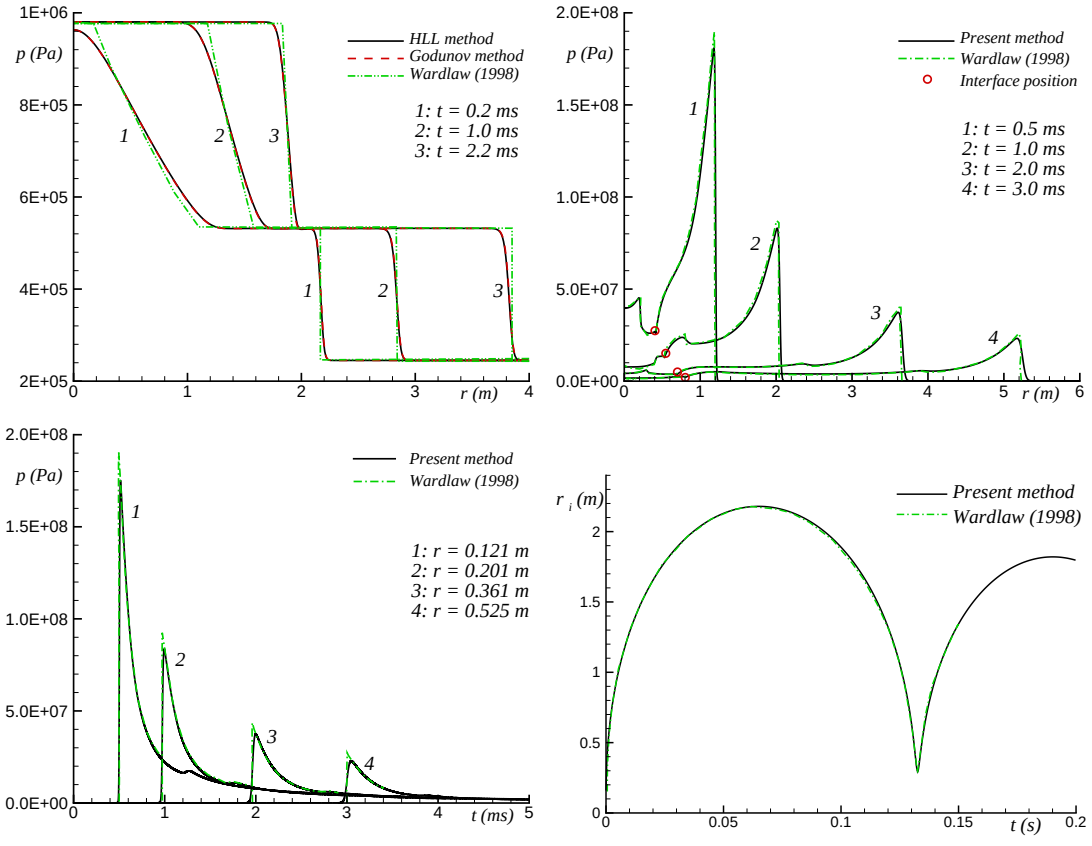

Figure 3. Top-left: case 1.A. Top-right and bottom-left: case 1.E. Bottom-right: case 1.F. The initial conditions for each case are given in table I.

DOI: 10.1002/nme

of the HLL Riemann solver is assessed in the top-left plot of the figure by comparing with a solver identical to the present but for using an exact Riemann solver for the fluxes (Godunov method). The case refers to a 1D problem with a single material, a γ-law gas. The HLL solver agrees with the Godunov method and has the advantage to be applicable for more general fluid conditions. The other shown numerical solution is obtained from a 3D method combining a fixed Cartesian grid with a Lagrangian approach in case of moving bodies and is documented in [15]. There, it is ensured the reliability of the 3D method which is applied to a systematic list of test cases to provide a reference solution for numerical verifications in connection with underwater explosions. In particular the examined problem corresponds to case 1.A in [15]. Except for a slightly smoother behavior near the interface, the present numerical results are consistent with those in [15]. The accuracy at large times is documented in the other plots of the figure referring to two cases of underwater explosions. Top-right and bottom-left of the figure refer to case 1E of [15] and examine the stage with a spherical explosion shock developing in the water. They give, respectively, the pressure distributions at four time instants and the pressure evolutions at four radial positions from the center of the bubble. The present method predicts correctly the evolution of the pressure in time, as well as the location of the advancing shock wave and of the gas-liquid interface, represented by the empty circles. The bottom-right figure is related to case 1F of [15] and considers the collapsing stage of the spherical bubble. Present results fit exactly the nonlinear behavior of the cavity oscillations reported in [15]. The initial conditions for the three cases in figure 3 are given in table I.

Case	r_i	Fluid Left	ρ_{0L}	p_{0L}	u_{0L}	Fluid Right	ρ_{0R}	p_{0R}	u_{0R}
1.A	2	$\gamma = 1.4$	2.0	$9.80 \cdot 10^5$	0	$\gamma = 1.4$	1.0	$2.45 \cdot 10^5$	0
1.E	0.16	JWL	1630.0	$7.80 \cdot 10^9$	0	$Water$	1000.0	$1.0 \cdot 10^5$	0
1.F	0.16	JWL	1630.0	$7.80 \cdot 10^9$	0	$Water$	1000.38	$1.0 \cdot 10^6$	0

Table I. Test cases from [15]. The data are given using SI system.

Prepared using nmeauth.cls
DOI: 10.1002/nme

Since the problem equation is hyperbolic, the radial solution can be applied in the real cases until the first shock wave from the explosion becomes close to the bottom of a vessel or another boundary. This is because the presence of the structure will not affect the fluid behind the shock wave. Once this wave reaches the boundary three-dimensional effects become important locally while radial symmetry is still preserved far from the boundary. This is the case when a zonal approach can be applied, as described next when the boundary is represented by a flat structure.

2.3. One-way time-space domain decomposition for compressible two-phase flows

As the shock wave becomes close to a body, a time-space domain-decomposition (DD) strategy is switched on, where the compressible 3D solver described in section 2.1 is initiated by the simplified radial solution given in section 2.2 within an inner region affected by the body and used to investigate the fluid-body interactions. The radial solution is still applied far from the structure and provides the boundary conditions to the 3D solver along a control surface bounding the inner domain. This implies a one-way coupling.

Figure 4 shows a sketch of the zonal strategy. The circular region gives the zone where the problem is radially symmetric and the radial solution is used, while the rectangular region represents the boundary of the 3D sub-domain. They have an overlapping layer where the solution is forced to go smoothly from the radial to the 3D behavior. In particular, the figure gives the dimensions of the zonal strategy used for the underwater explosion examined in section 3.3. The radial solution is used within the circular domain, up to a distance of 1m -4Δx_{loc} from the bubble center. Here Δx_{loc} is the local size in the 3D sub-domain. Within the radial layer of 4 Δx_{loc} from this distance, the problem is solved both using the radial solver and the 3D method and the numerical solution is forced to smoothly go from the radial to the 3D solution. For larger distances, the 3D solution is applied. The developed DD limits the computational costs which are quite high if a compressible 3D solver is used for the whole simulation and everywhere due to the limits in the time step connected with the local speed of sound in the fluid. If the explosion occurs sufficiently close to boundaries, such as the free surface, the sea floor or vehicles, then three-dimensional effects are important since the beginning and this DD cannot be applied. In this case, the 3D numerical solver described in section

Prepared using nmeauth.cls
DOI: 10.1002/nme

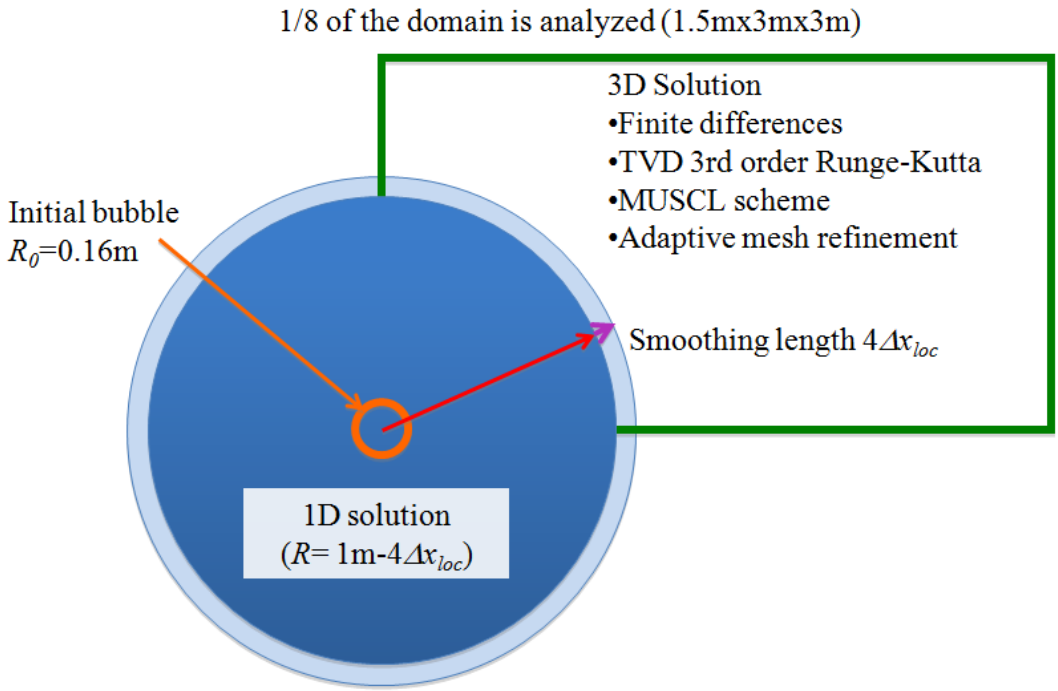

Figure 4. Radial-3D domain decomposition strategy with the values used in the underwater-explosion problem discussed in section 3.3.

2.1 must be used for the whole simulation. This means a computational cost and a memory space increasing with a factor

$$\frac{\alpha N + (1-\alpha)N^3}{N} \tag{5}$$

where α is the fraction of the domain solved with rally symmetric 1D solution and N is the number of points per characteristic length.

2.4. Structural modeling: orthotropic plate and coupling with fluid-dynamic problem

In a first attempt to estimate the local effects on the bottom of a vessel, this has been modelled as a rectangular orthotropic plate with length L and width B in x and y direction, respectively. The plate is assumed to undergo linear deformation $w(x, y, t)$ governed in time and space by the equation

$$m\frac{\partial^2 w}{\partial t^2} + D_x\frac{\partial^4 w}{\partial x^4} + 2BB\frac{\partial^4 w}{\partial x^2 \partial y^2} + D_y\frac{\partial^4 w}{\partial y^4} = p(x, y, w, t)\,. \tag{6}$$

Here m is the average plate mass per unit area, D_x and D_y are its flexural rigidities in the two main directions and BB is its effective torsional rigidity (see *e.g.* [16]). On the right-hand-side, p

Prepared using nmeauth.cls
DOI: 10.1002/nme

is the local hydrodynamic pressure acting on the plate which depends on the space, time w and, in particular, on its time derivatives. If the DD strategy is considered, p is obtained by solving the fluid-structure coupled problem, *i.e.* the mentioned dependence on the derivatives of w is implicit. If the radial solution is used to simulate the incident acoustic wave, p is modelled as

$$p(x, y, w, t) = 2P_i(r, t) - \frac{\rho c}{\cos(\theta)} \frac{\partial w}{\partial t} + \text{added-mass contribution.} \tag{7}$$

Here P_i is the incident wave pressure, c is the speed of sound and θ is the angle between the direction of the incident wave reaching locally the plate and the plate normal vector (see left sketch in figure 5). The first two terms on the right-hand side represent the sum of the incident

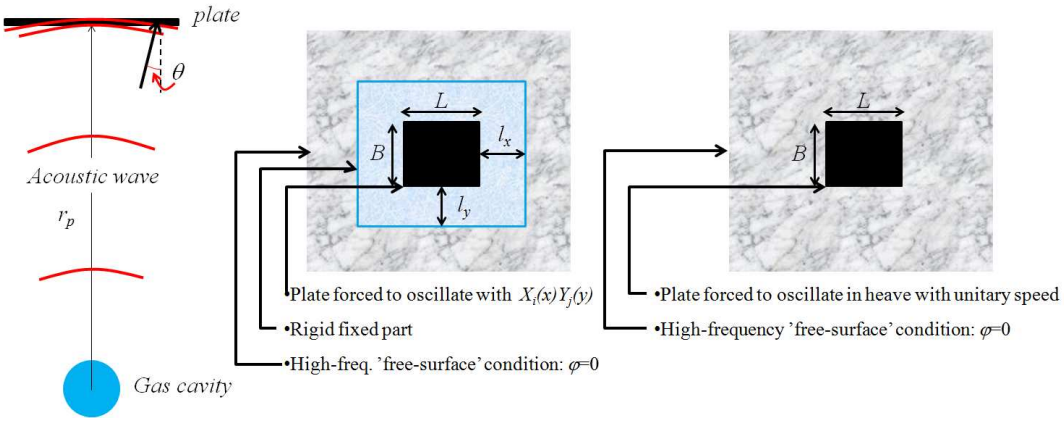

Figure 5. Left: radial acoustic waves reaching a plate and definition of the angle θ. Center: problem solved with a BEM to find the added masses for the elastic modes. Right: problem solved with a BEM to find the heave added mass for the plate.

and reflected wave from the wall leading to twice P_i for a fixed wall 'plus' an acoustic wave-radiation damping in the case of rigidly moving or deformable plate. They act during the acoustic phase, *i.e.* when compressibility matters also for the liquid. The last term, not written explicitly, is an incompressible added-mass contribution which matters when the water behaves as incompressible and the plate oscillates as a consequence of the interaction with the incident acoustic wave. In the present implementation the acoustic wave-radiation damping term is switched off when P_i becomes half of the acoustic pressure associated with the incident wave, *i.e.* if $P_i \leq \rho c U_i$, with U_i the radial velocity of the incident wave. The added-mass term is used during the whole simulation. This

Prepared using nmeauth.cls
DOI: 10.1002/nme

contribution is estimated in an approximated way studying the radiation problem for each plate mode and assuming that the plate is surrounded by a fixed wall and then by a flat 'free surface' with velocity potential $\varphi = 0$ (see center sketch in figure 5). This means that it is a high-frequency added mass estimation. Obviously this is an approximation because in the real case of a ship, the plate is used to simulate the grillage on the bottom so the free surface will be not aligned with the plate. The surrounding fixed wall is used to avoid a pure Neumann problem which would lead to a solution in general dependent on an arbitrary constant. The dimensions of the fixed wall are assumed large enough so that increasing them there is practically no influence on the added mass. It was found that an extension along x, say l_x, $\geq 4L$ and along y, say l_y, $\geq 4B$, was enough. So to limit the computational costs, a uniform mesh was used within a zone with similar extensions as the elastic plate and then a stretching was introduced to have a fixed-wall zone larger than the minimum required dimensions. The stretching was continued also on the 'free surface'. Numerical convergence of the added-mass results was ensured by successive refinement.

B/L	Form. 1	Meas. 1	Form. 2	Form. 3	Meas. 2	Pot. Sol.	Present Sol.
0.1	0.950		0.953	0.995		0.947	0.971
0.5	0.750	0.733	0.742	0.895	0.911	0.757	0.763
1.0	0.500	0.565	0.557	0.707	0.694	0.579	0.583

Table II. Infinite-frequency added mass in heave for a plate. Here 'Form.' refers to an empirical formula, 'Meas.' to experimental results, 'Pot. sol.' to the potential-flow solution based on a dipole-distribution on the plate in [24]. The results are presented in the same order as in table 3 in [24]. The numbers correspond to the nondimensional added mass $A^*_{33} = A_{33}/[\pi\rho(0.5B)^2 L]$.

Verifications and validations of the Boundary Element Method (BEM) developed to estimate the added masses are presented in table II and figure 6, respectively, for the case of infinite-frequency added-mass in heave for a plate surrounded by an infinite flat free surface (see right sketch in figure 5) and for the added masses of the elastic modes for a plate as discussed above. In the case of the heave, the present results tend to provide slightly large values but comparable and close to the other

Prepared using nmeauth.cls
DOI: 10.1002/nme

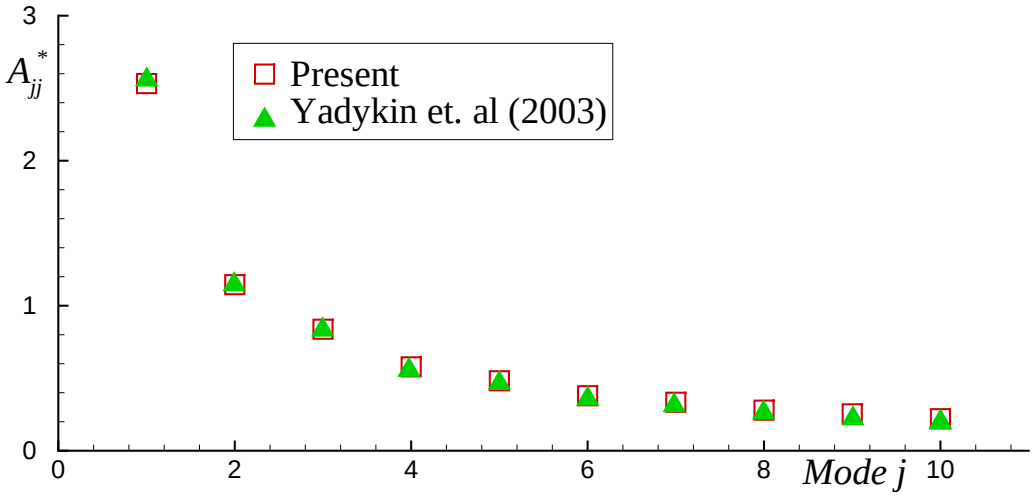

Figure 6. Added mass for the elastic modes of a simply-supported uniform plate: present results and solution from [25]. $A^*_{jj} = \pi A_{jj}/(\rho B L^2)$.

reference solutions. For the elastic modes, they fit well the reference numerical solution based on energy considerations and estimation of the pressure jump across the plate.

3. APPLICATIONS

Here the problem of underwater explosions with structures is examined to assess the potentiality of the different parts of the solver and to carry on a more detailed physical investigation.

3.1. Radial acoustic waves interacting with a uniform plate

The underwater explosions studied experimentally and numerically in [17] for uniform steel restrained plates is examined here to verify the implementation of the solver as radial incident acoustic waves and elastic plate and to check the reliability limits of the linear model for the structure. The experiments examined a plate at different distances r_p from a charge and also varied the charge weight W. The combination of these parameters may lead to plastic deformations and to the rupture of the plate. In this framework a relevant parameter is the shock factor defined in [17] as $SF = 0.45\sqrt{W}/r_p$. Here we examine two cases with charge weight $W = 0.005$ Kg and minimum plate distances $r_p = 0.50$ and 0.15 m. These two conditions correspond to $SF = 0.064$ and 0.212 $\sqrt{\text{Kg}}$/m, respectively, and led experimentally to a limited and a more pronounced plastic

Prepared using nmeauth.cls
DOI: 10.1002/nme

deformation of the plate, respectively, without rupture of the structure. This means that strictly speaking we are outside the range of applicability of our linear plate modelling. According to [17] the maximum incident wave pressure in the two cases was about 16.45 and 63.55 MPa, respectively. So the underwater-explosion radial solution was designed to achieve these maximum values at the plate location for the two cases. Left plot of figure 7 shows the time evolution of the deformation at the center of the plate as obtained by the present orthotropic plate and by the Finite Element Method (FEM) in [17] when assuming linear behavior of the structure for the case with $r_p = 0.50$ m. Since no added-mass contribution is accounted for in [17], also our results consider only the

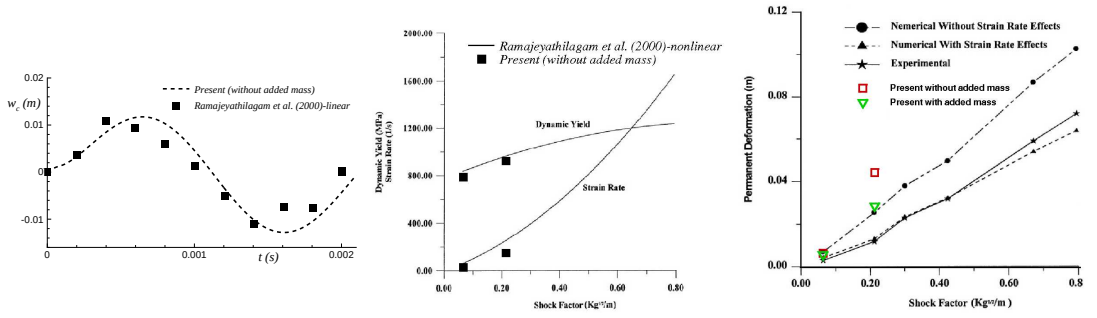

Figure 7. Underwater explosion studied in [17]. Left: evolution of the plate deformation at the center of the plate for $r_p = 0.50$ m. Center: maximum strain rate and dynamic yield stress obtained from empirical expression (8). Right: plastic deformation as obtained by experiments and numerics in [17] and present results without and added mass effects. The center and right figures are original figures from [17] with present results added.

acoustic-load contributions. The agreement is fairly good both in terms of amplitudes and of time scales of oscillations. This is very promising considering the differences between the two structural solution methods, as well as between the incident wave pressures in our case simulated by the radial solver and in [17] estimated from a classical empirical formula based on the underwater-explosion studies reported for instance in [2]. The center plot of figure 7 examines the dynamic yield stress σ_{dy} as a function of the shock factor. σ_{dy} is obtained using the empirical Cowper-Symonds formula

Prepared using nmeauth.cls
DOI: 10.1002/nme

(see [18])

$$\sigma_{dy} = \sigma_y(1 + |\dot{\epsilon}/D|^{1/n}) \tag{8}$$

with σ_y the static yield stress and D and n two empirical material parameters. In the present case of high-strength steel, $\sigma_y = 400$ MPa, $D = 40/s^{-1}$ and $n = 5$. This formula states that the dynamic yield stress becomes larger than the static value due to effects of the strain rate $\dot{\epsilon}$ on the constitutive properties of the material. Present σ_{dy} results for the two examined cases have been obtained for a simulation, after the impact, as long as the reference results and then estimating σ_{dy} from the maximum $\dot{\epsilon}$ recorded. Also in this case the agreement is quite good suggesting similar deformations of the plate in time. The right of figure 7 examines the plastic deformation as measured in the model tests of [17] and as numerically predicted with a nonlinear structural model accounting or not for the change of the dynamic stress due to the strain rate effects. In our case the prediction of the plastic deformation is roughly obtained as the difference between the maximum recorded deformation on the plate and the maximum elastic deformation. The latter is estimated as the maximum deformation of the plate for maximum stress smaller than or equal to the instantaneous dynamic yield stress. The comparisons show that our predictions are consistent for $SF = 0.064$ with the nonlinear-structural numerical results in [17] without strain-rate corrections. This is reasonable in this case because the plate has a very limited plastic deformation and so the elastic deformation dominates. Present results overpredict much the plastic deformation for $SF = 0.212\ \sqrt{\text{Kg}}/\text{m}$ because in this case the variations in the structural properties of the steel plate are important both in terms of nonlinear stress-strain constitutive link and of the temporal increase of the dynamic yield stress. It is interesting to note that when including the incompressible added-mass effects the estimation ameliorates and becomes very close to the nonlinear solution without strain-rate effects.

The plastic regime is out of the scope of the present work but its analysis here is interesting because it has shown that within a certain limit the elastic plate modelling is able to provide a rough estimate of onset and value of plastic deformations.

Prepared using nmeauth.cls
DOI: 10.1002/nme

3.2. Radial acoustic waves interacting with a navy ship bottom

Here the radial solution for the underwater explosion in infinite liquid is used to investigate the possible consequences on the bottom of a navy ship as a function of its minimum distance r_p from the initial charge. The bottom grillage arrangement is chosen as the configuration 1a among those studied experimentally in [19] (see sketch in figure 8) and an equivalent orthotropic plate was obtained extended as the grillage and restrained at all edges. The parameters of the equivalent plate

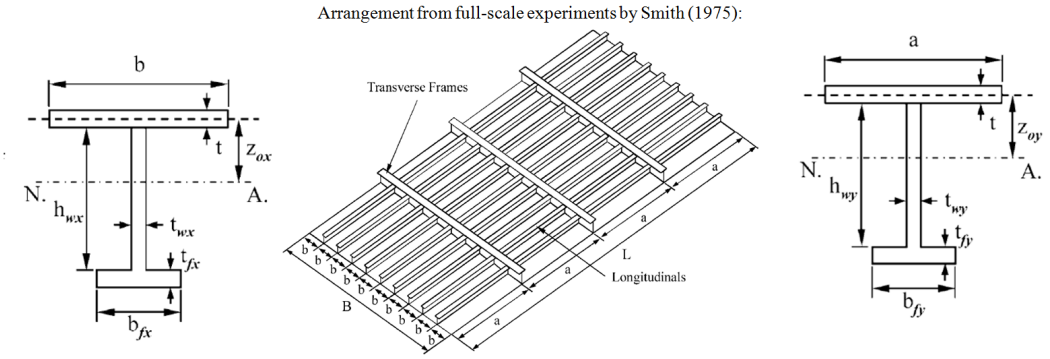

Figure 8. Steel-grillage arrangement for bottom of navy ships as studied experimentally in [19]. Here L and B are the longitudinal and transversal length of the grillage, respectively, a and b are the distance between two transverse frames and two longitudinal stiffeners, respectively. In the present case, grillage 1a with 4 transverse frames and 4 longitudinal stiffeners is examined. The parameters are $L = 6.096$ m, $B = 3.048$ m, $t = 0.008$ m, $h_{wx} = 0.15367$ m, $t_{wx} = 0.00721$ m, $b_{fx} = 0.07899$ m, $t_{fx} = 0.01422$ m, $h_{wy} = 0.25756$ m, $t_{wy} = 0.00937$ m, $b_{fy} = 0.12548$ m, $t_{fy} = 0.01829$ m.

are given in table III.

L	B	m	D_x	D_y	BB	σ_y
6.069	3.048	85.785	$1.262{\cdot}10^7$	$3.517{\cdot}10^7$	$2.614{\cdot}10^4$	$250.4{\cdot}10^6$

Table III. Equivalent orthotropic plate for the steel-grillage arrangement 1a of [19] documented in figure 8. The values are given SI system. L and B are the plate extensions in x and y direction, respectively. σ_y is the yield stress of the plate.

Prepared using nmeauth.cls
DOI: 10.1002/nme

The underwater explosion documented in [20] has been considered as test case since it is rather used as sample of explosion to assess possible ship damages. The initial radius of the gas cavity is $R_0 = 0.16$ m and the parameters for the EOS of the fluids, using SI system, are: $\rho_{0g} = 1630.0$, $p_{0g} = 8.381 \cdot 10^9$, $A_g = 3.712 \cdot 10^{11}$, $B_g = 3.23 \cdot 10^9$, $R_1 = 4.15$, $R_2 = 0.95$, $\omega = 0.30$, $\rho_{0w} = 1025.0$, $p_{0w} = 1.0 \cdot 10^6$, $A_w = 1.0 \cdot 10^6$, $B_w = 3.31E8$ and $\gamma_w = 7.5$.

A convergence analysis of the radial solver has been performed using a computational domain 10 m long and a uniform radial discretization Δr. The order of accuracy OA (see [21]) was adopted as measure, which involves the time integral of the selected variable calculated with three discretizations and should be one for a solver accurate to the first order as in the present implementation. In our case, using $\Delta r = 0.00125$ m, $1.5\Delta r$ ant $2.25\Delta r$ and studying the evolution up to 0.05 s, at a location $r \simeq 44R_0$, OA was 1.45, 1.44, 1.32 and 1.56, respectively for u, p, ρ and E. At the interface OA is more limited and was found 0.39, 0.80 and 1.10, for the position of the interface, r_i, and for u_i and p_i, respectively. This is because across the interface complex phenomena occur, such as wave reflections and transmissions and generally large variable changes.

The evolution for the finest grid is shown in figure 9 in terms of pressure, velocity and density distributions and interface location at different time instants during the initial shock-wave phase. This stage involves a cavity expansion and is typically associated with a release of more than 50% of the energy from the explosion (see [22]). In this example, at first (left plots) a primary shock wave is caused by the detonation and moves away from the cavity while an expansion wave propagates toward the bubble center lowering the pressure, the velocity and the density inside the cavity. As time goes on, the expansion wave is reflected from the bubble center and the inner pressure rises again moving in the form of a shock wave towards the interface. There, it is partially reflected and partially transmitted into the liquid phase (center plots). As a consequence of these repeated reflections, the strength of the involved shock waves reduces in time and compressible effects become less important in the liquid (right plots). The described results fit well with the reference numerical solution in [20], based on an arbitrary Lagrangian-Eulerian version of the advective upstream-splitting shock-capturing scheme, also given in the figure. This confirms again the accuracy of the

Prepared using nmeauth.cls
DOI: 10.1002/nme

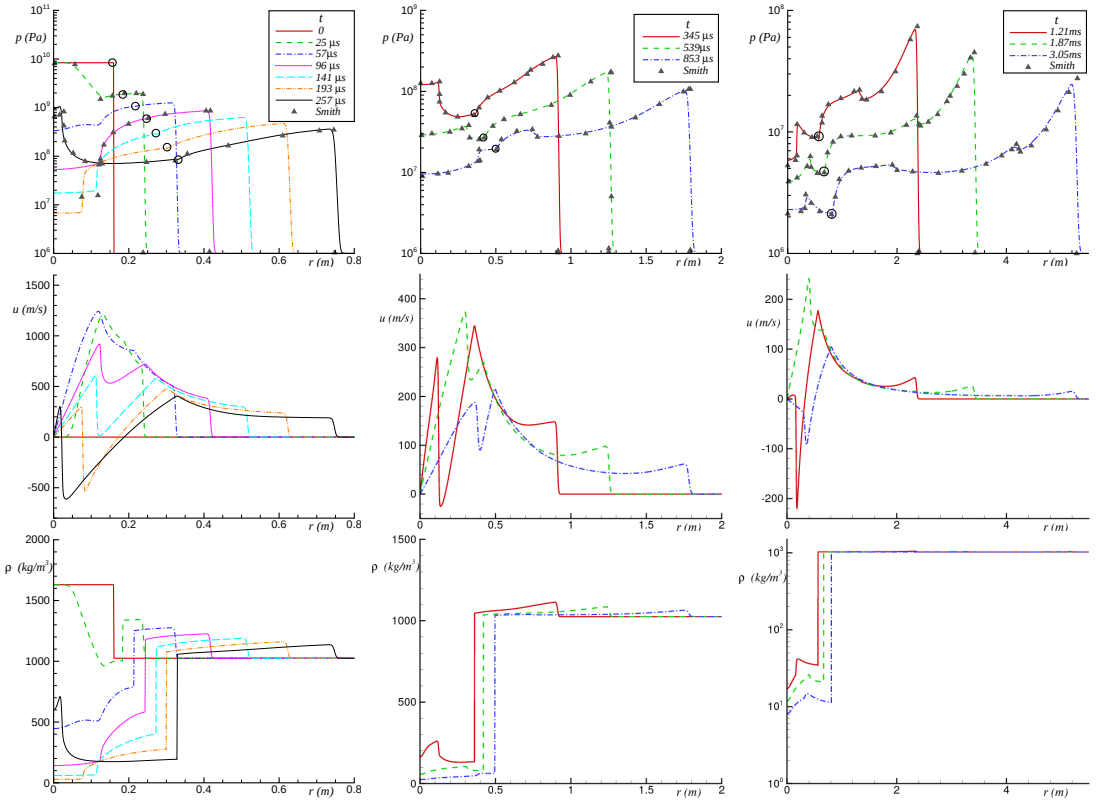

Figure 9. Present radial solution for the underwater explosion in [20]: pressure (top), radial velocity (center) and density (bottom) distributions at different time instants. The empty circles indicate the instantaneous radial location of the interface. The triangles are the pressure numerical results in [20]. For sake of clarity, in the left plot only the Smith's solutions at 25, 96 and 257μs, are shown.

developed method. On a longer time scale the cavity reaches a maximum radius of about 2.2 m ($\simeq 13.8R_0$) at about 0.066 s, this is consistent with the values reported in [20]. Then, within the gas-bubble phase, the cavity starts to oscillate with smaller amplitudes as shown in the left of figure 10. Both pressure and velocity at the interface (center and right plots) are highest at the beginning. When the bubble is compressed the pressure tends to a peak and the velocity becomes negative, both their magnitudes decreasing in time. According to studies in [22], most of the remaining energy from the explosion is released during the first bubble pulsation.

The equivalent orthotropic plate described above is introduced at a distance $r_p = 35$ m, 8 m and 4 m from the initial explosion to check possible consequences on the bottom of a navy vessel. It

Prepared using nmeauth.cls
DOI: 10.1002/nme

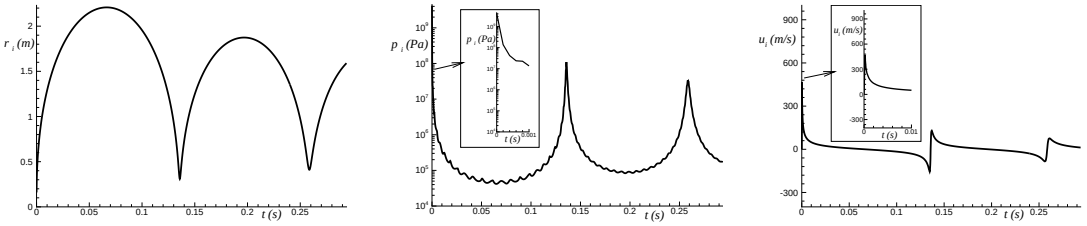

Figure 10. Present radial solution for the underwater explosion in [20]: location (left), pressure (center) and radial velocity (right) of the interface as a function of time. The results were obtained using a computational domain long 100 m, with constant $\Delta r = 0.00125$ m within 10 m and then stretching exponentially outwards.

is assumed that the center of the plate is the first location reached by the acoustic waves which, as time goes on, meet other parts of the structure. The numerical results are given in figure 11 in terms of the evolution of the maximum stress in the x direction on the plate, occurring at the middle in this case. For the largest distance r_p, the maximum stress is smaller than the yield stress and the

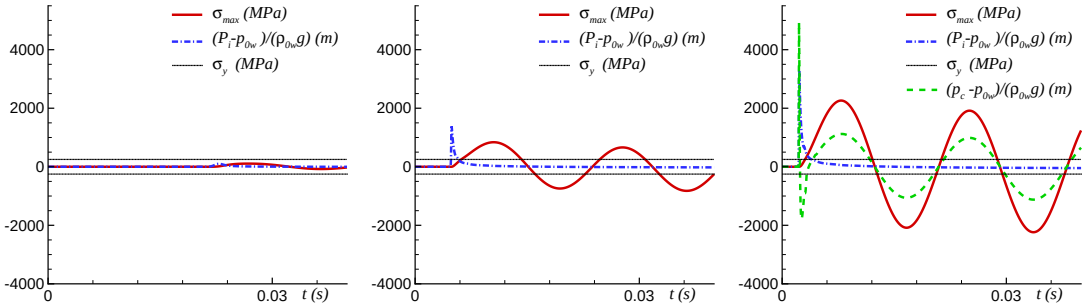

Figure 11. Evolution of the maximum stress on the plate for minimum plate distance $r_p = 35$ m, (left) 8 m (center) and 4 m (right). P_i, p_{0w} and p_c are the incident pressure at the center of the plate, the ambient pressure in water (without hydrostatic pressure) and the pressure at the center of the plate, respectively. σ_y is the yield stress of the plate.

plate will deform elastically with a period depending on the mass and elastic-mode added mass. For $r_p = 8$ m, plastic deformation seems likely to occur and it will be more pronounced for $r_p = 4$ m. In the latter case, there will be also danger for plate rupture. To quantify the plastic deformation, as well as to predict reduction of plate thickness and damage of the ship bottom, the method must be extended. An extension is also necessary for other reasons. The pressure on the body becomes rather lower than the atmospheric pressure (the pressure at the center of the plate is the dashed line on the

Prepared using nmeauth.cls
DOI: 10.1002/nme

right plot). It means that when adding the hydrostatic pressure at the ship bottom, the total pressure is likely to be negative. This cannot happen in reality, when the pressure becomes close to the vapor pressure, cavitation will occur locally with liquid becoming vapor. The occurrence of cavitation and the further stages of the fluid-body interactions require a more general method. In figure 11 also the incident pressure at the center of the plate is reported and indicates a loading duration much shorter than one-fourth of the highest natural period of the structure. This means that the plate undergoes a first short inertial phase followed by a free-vibration phase, similarly as described in [23], if the plate is not damaged and the elastic deformation is not negligible.

3.3. 3D acoustic waves interacting with a rigid plate

The developed DD is applied as explained in section 2.3 to the same underwater-explosion problem examined in section 3.2 by assuming an infinite wall at a radial distance of 1.5 m from the center of the bubble. The 3D sub-domain actually used for the simulation is shown in the left of figure 12 at a

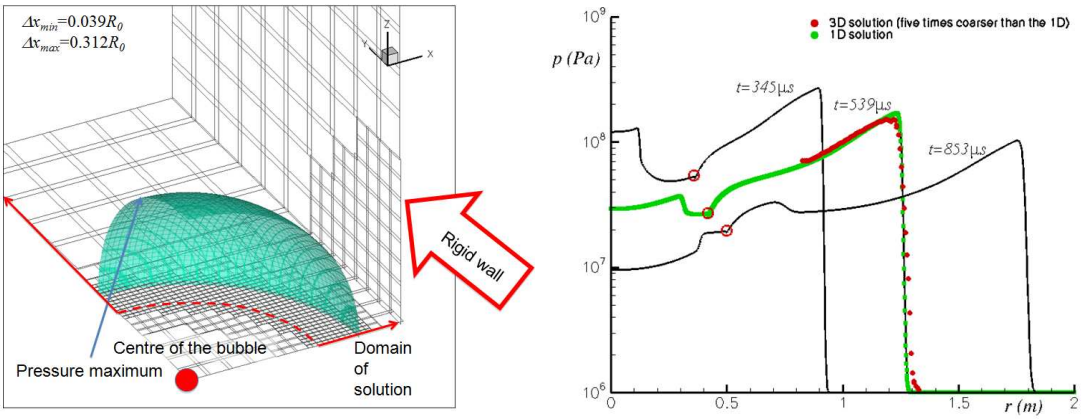

Figure 12. Left: Radial-3D domain decomposition strategy with maximum pressure location at the initial time of the DD, instantaneous mesh and rigid wall. Right: pressure distribution in radial direction from the full radial solution and from the DD solution in the 3D sub-domain.

certain time instant during the evolution. The figure also shows the domain where the radial solution is used and provided to the 3D solution. The mesh is well refined near the surface of maximum pressure and becomes coarse sufficiently far from the zone where important flow evolution occurs. The 3D solution for the acoustic incident wave to the rigid wall is given in the right side of figure 12

Prepared using nmeauth.cls
DOI: 10.1002/nme

in terms of radial pressure distribution at time $t = 0.539$ ms and compares well with the full radial solution also reported. A close view of the 3D solution near the zone of large pressure variation highlights some small oscillations. These represent a draw-back of using the superbee limiter (see *e.g.* [21]) for the variable fluxes to keep sufficiently sharp the flow gradients. The oscillations remain limited in time but a more suitable limiter will be considered in the future as improvement of the solution method.

The acoustic wave evolution and its interaction with the wall is examined in figure 13 in terms of the pressure and maximum density iso-surfaces evolution. As expected the level of the pressure reduces in time as the acoustic wave propagates and the density iso-surfaces maintain the radial symmetry until the acoustic wave reaches the wall. There, the wave is reflected with a local rise of the pressure and a full 3D character of the solution near the wall which enlarges as time goes on.

Figures 14 and 15 summarize the advantage of using the adaptive mesh refinement for this kind of problems. Two simulations have been carried out: one is obtained with the dynamic mesh algorithm, refining the mesh where density exceed a threshold value and one with a fixed mesh with four levels of discretizations for the mesh blocks. This means that the two simulations have similar local mesh size in the zones of large pressures. The adaptive mesh increases the number of nodes as the simulation goes on while the fixed mesh has the same high loading cost for the whole simulation. As a result there is a much larger memory-space requirement and a factor of about 1.6 in terms of computational time for the same physical time interval simulated. Another important advantage of the adaptive mesh algorithm is a smoother and more robust solution. This can be seen in a slice of the pressure solution (figure 14) and in the surface with maximum pressure (figure 15) at a time instant during the wave reflection stage from the wall. The fixed mesh gives an unphysical smeared behavior of the pressure, when the mesh becomes too coarse. This is because in the fixed mesh the discretization remains as it is and it might be not sufficiently fine from time to time during the evolution. The 3D solver with adaptive-mesh algorithm is able to capture correctly the wave reflection from the rigid wall and predicts a maximum wall pressure twice the incident wave pressure.

Prepared using nmeauth.cls
DOI: 10.1002/nme

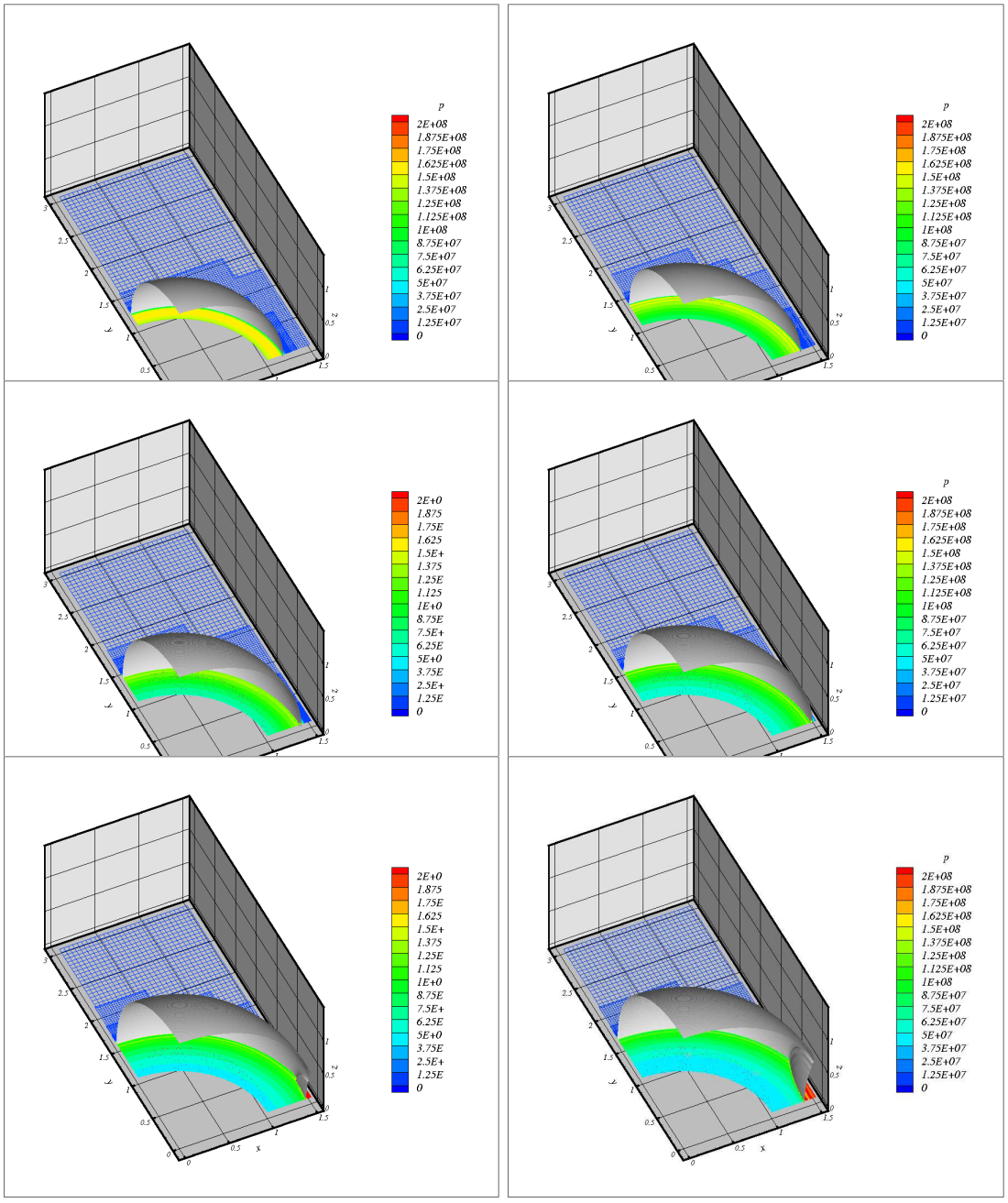

Figure 13. Time evolution of the pressure at the centreplane and density iso-surfaces maximum ρ on the line $x = 0$ and $z = 0$. Time increases from left to right and from top to bottom and corresponds to about 0.480, 0.570, 0.615, 0.660, 0.705 and 0.750 ms.

Prepared using nmeauth.cls
DOI: 10.1002/nme

	Adaptive Mesh Refinement	Fixed Mesh on 4 levels
Computational time on 24 2300MHz processors	6h 10 min	10h 40min
Size	From 0.45 to 8.8 Mil points	8.5 Mil points

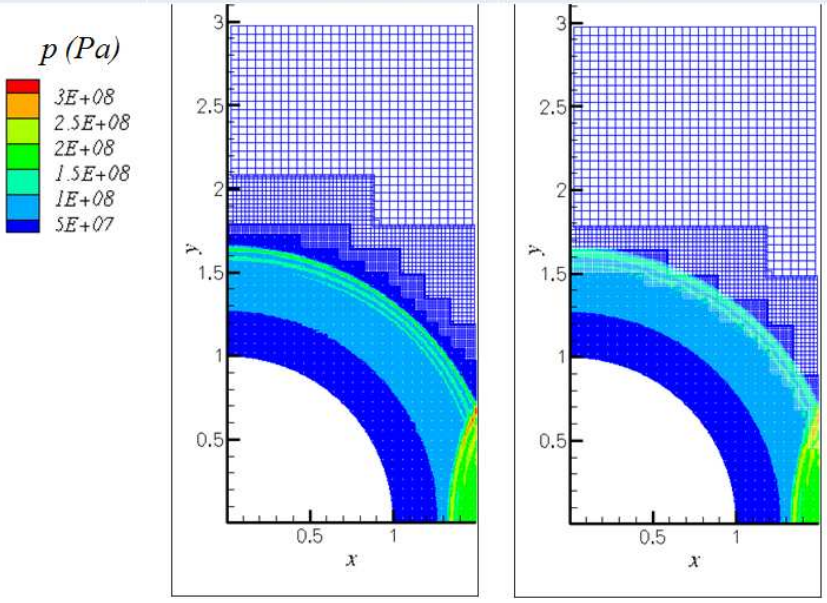

Figure 14. Adaptive mesh versus fixed discretization: CPU-time and memory requirements, and snapshot of a pressure solution.

Adaptive Mesh Refinement	Fixed Mesh on 4 levels

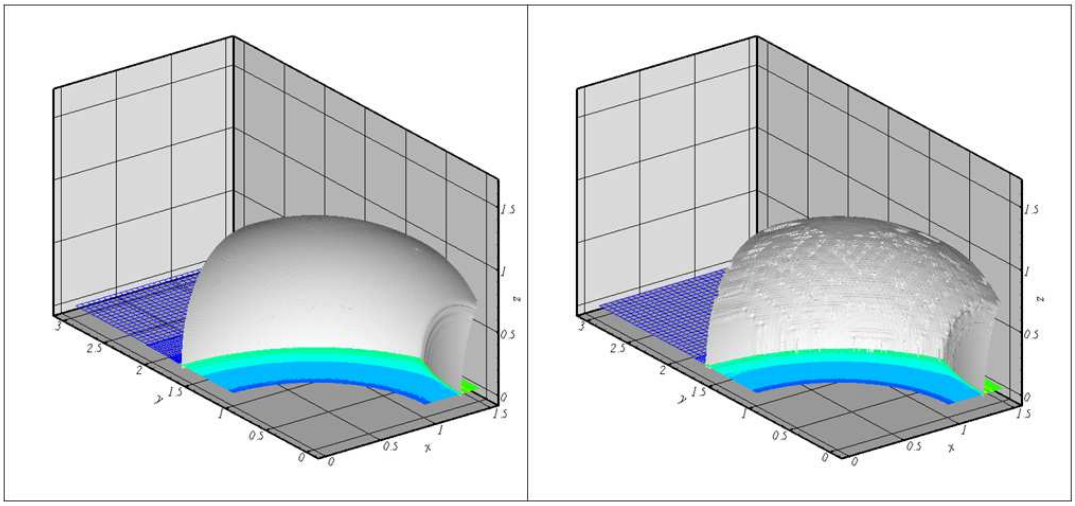

Figure 15. Adaptive mesh versus fixed discretization: snapshot of the surface with maximum pressure.

Prepared using nmeauth.cls
DOI: 10.1002/nme

4. CONCLUSIONS

The problem of gas cavities surrounded by liquid and interacting with structures is investigated. The aim is to achieve a solver able to predict the cavity evolution from the acoustic phase until the cavity oscillation phase and so to switch from a compressible to an incompressible solver for the liquid phase. Presently only the compressible phase has been focused on, but the later stage was already examined in [6] so the inclusion of this evolution phase should be manageable. A numerical domain-decomposition (DD) strategy has been proposed as a compromise between capability, accuracy and efficiency. It is characterized by a one-way coupling from a radial compressible solution to a 3D compressible solution. The 3D solver is based on a finite-difference scheme and applies an adaptive mesh algorithm to ensure proper refinement when and were necessary. The different parts of the solver have been assessed and physical analyses carried out for the underwater-explosion cases examined.

The next steps of the research concern the further development of the DD. To make more flexible and efficient the solver it is useful that not only the mesh is adaptive but also the extension of the 3D sub-domain so to account for the three-dimensional effects when and where necessary. The deformability of the structure must be accounted for in the 3D solver, but this is an easier extension of the method.

ACKNOWLEDGMENTS

This research activity is partially funded by the Centre for Autonomous Marine Operations and Systems (AMOS), NTNU, Norway, and partially by the Flagship Project RITMARE - The Italian Research for the Sea - coordinated by the Italian National Research Council and funded by the Italian Ministry of Education, University and Research within the National Research Program 2011-2013.

REFERENCES

Prepared using nmeauth.cls
DOI: 10.1002/nme

1. Brown A.J. *AOE 5315 Naval Ship Vulnerability and Underwater Explosion - Introduction to Survivability OnLine Lecture 1*. Virginia Tech Department of Aerospace and Ocean Engineering. 2004.
2. Cole R.H. *Underwater Explosions* Princeton, New Jersey: Princeton University Press. 1948.
3. Dular M. and Coutier-Delgosha O. Numerical modelling of cavitation erosion *Int. J. of Numerical Methods in Fluids.* 2009; **61** (12): 1388-1410.
4. Watanabe T., Maehara H. and Itoh S. Basic study on promotion of thawing frozen soil by shock loading. *Int. J. of Multiphysics.* 2008; **2** (2): 155-163.
5. Lingeman J.E. McAteer J.A., Gnessin E. and Evan A.P. Shock wave lithotripsy: advances in technology and technique. *Nat. Rev. Urol.* 2009; **6**: 660-670.
6. Colicchio G., Greco M. and Faltinsen O.M. Domain-Decomposition Strategy for Marine Applications with Cavities Entrapments. *J. of Fluids and Structures.* 2011; **27** (4): 567-585.
7. Colicchio G., Greco M. and Faltinsen O.M. A numerical strategy for gas cavity-body interactions from acoustic to incompressible liquid phases. 28^{th} *Int. Workshop of Water Waves and Floating Bodies.* 2013; pp. 4.
8. Colicchio G., Greco M., Faltinsen O.M. and Brocchini M. Gas cavity-body interactions: efficient numerical solution. *EURO 555.* 2013.
9. Dobratz B. M. and Crawford P. C. *LLNL Explosives HandbookProperties of Chemical Explosives and Explosive Simulants.* Lawrence Livermore National Laboratory. 1985.
10. Shu C.W. and Osher S. Efficient implementation of essentially non-oscillatory shock-capturing schemes. *J. Comput. Phys.* 1988; **77**: 439-471.
11. Van Leer B. Towards the ultimate conservative difference scheme V. A second order sequel to Godunovs method. *J. Comput. Phys.* 1979; **32**: 101-136.
12. Liu T.G., Khoo B.C. and Yeo K.S. Ghost fluid method for strong shock impacting on material interface. *J. Comput. Phys.* 2003; **190**: 651-680.
13. MacNeice P., Olson K.M., Mobarry C. , deFainchtein R. and Packer C. PARAMESH : A parallel adaptive mesh refinement community toolkit. *Computer Physics Communications.* 2000; **126**: 330-354.
14. Toro E.F. *Riemann Solvers and Numerical Methods for Fluid Dynamics.* Springer-Verlag. 1999.
15. Wardlaw A.B. *Underwater explosion test cases.* Naval Surface Warfare Center. 1998; **ADB238684**.
16. Faltinsen O.M. Water entry of a wedge by hydroelastic orthotropic plate theory. *J. Ship Research.* 1999; **43** (3): 180-193.
17. Ramajeyathilagam K., Vendhan C.P. and Bhujanga Rao V. Non-linear transient dynamic response of rectangular plates under shock loading. *J. of Impact Engineering.* 2000; **24**: 999-1015.
18. Jones N. *Structural impact.* Cambridge: Cambridge University Press. 1989.
19. Smith C.S. Compressive strength of welded steel ship grillages. *Trans. Roy. Inst. Naval Archit.*. 1975: 325-359.
20. Smith R.W. AUSM(ALE): A Geometrically Conservative Arbitrary LagrangianEulerian Flux Splitting Scheme. *J. of Computational Physics*. 1999: 268-286.

Prepared using nmeauth.cls
DOI: 10.1002/nme

21. Colicchio G. Violent disturbance and fragmentation of free surfaces. *Ph.D. thesis*. University of Southampton,Southampton, UK. 2004.
22. Keil A.H. *The response of ships to underwater explosions.* David Taylor Model Basin. 1961; **1576**.
23. Faltinsen O.M. *Hydrodynamics of High-Speed Marine Vehicles.* Cambridge University Press, Cambridge, UK. 2005.
24. Meyerhoff W.K. *Die Berechnung hydroelastischer Stosse.* Schiffstechnik. 1965; **12** (60): 18-30.
25. Yadykin Y., Tenetov V. and Levin D. The added mass of a flexible plate oscillating in a fluid. *J. of Fluids and Structures.* 2003; **17**: 115-123.

Prepared using nmeauth.cls
DOI: 10.1002/nme